Supplementary Information (SI) for Journal of Materials Chemistry A.
This journal is © The Royal Society of Chemistry 2024

Electronic Supplementary Information

Enhanced indoor photovoltaic efficiency of 40% in dye-sensitized solar cells using cocktail starburst triphenylamine dyes and dual species copper electrolyte

Paravakkal Ramees Jebin,[ac] Andrew Simon George,[ac] Rakesh K. Mishra,[d] Jubi John,*[bc] and Suraj Soman*[ac]

[a]Centre for Sustainable Energy Technologies, CSIR-National Institute for Interdisciplinary Science and Technology (CSIR-NIIST), Thiruvananthapuram 695019, India. Email: suraj@niist.res.in
[b]Chemical Sciences and Technology Division, CSIR-National Institute for Interdisciplinary Science and Technology (CSIR-NIIST), Thiruvananthapuram 695019, India.
[c]Academy of Scientific and Innovative Research (AcSIR), Ghaziabad-201002, India.
[d]Department of Chemistry, National Institute of Technology Uttarakhand (NITUK), Srinagar, Garhwal 246174, India.

TABLE OF CONTENTS

S. No.	Experimental Details	Page No
Section-I	**Materials**…… ……...	4
Section-II	Experimental procedure for the synthesis of **RJ-C6** dye……...	5
	Synthesis of 4-(diphenylamino)benzaldehyde (**2**)……..	5
	Synthesis of 4-(bis(4 iodophenyl)amino)benzaldehyde (**3**)……...	5
	Synthesis of 1,3-bis(hexyloxy)benzene (**5**)…….....	6
	Synthesis of 2,4-bis(hexyloxy)-1-iodobenzene (**6**)…….....	6
	Synthesis of ((2,4-bis(hexyloxy)phenyl)ethynyl)trimethylsilane (**7**)……..	7
	Synthesis of 1-ethynyl-2,4-bis(hexyloxy)benzene (**8**)……	7-8
	Synthesis of 4-(bis(4-((2,4-bis(hexyloxy)phenyl)ethynyl)phenyl)amino)benzaldehyde (**9**)….....	8
	Synthesis of 3-(4-(bis(4-((2,4-bis(hexyloxy)phenyl)ethynyl)phenyl)amino)phenyl)-2-cyanoacrylic acid (**RJ-C6**)…… ……	9
Section-III	**Fig. S1-S10:** ^{1}H NMR, and ^{13}C NMR spectra of precursors (**2**-**9**) and **RJ-C6** dye.....	10-14
Section-IV	**Dye loading**…… …….....	15
Section-V	**Theoretical studies of the dyes**……..	16
	Table S1 : Dihedral angles of **L0, DNF-13**, and **RJ-C6**……	16
	Fig. S11 : Side view of the dyes **L0**, **DN-F13**, and **RJ-C6** …….....	16
	Fig. S12 : The length of the molecules **L0**, **DN-F13**, **RJ-C6** and **XY1b**……..……..	17
	Table S2 : TD-DFT calculated prominent electronic transitions of **L0**……	18
	Table S3 : TD-DFT calculated prominent electronic transitions of **DN-F13**….....	19
	Table S4 : TD-DFT calculated prominent electronic transitions of **RJ-C6**….....	20

Section-VI **Device fabrication and characterization**……..... 21-22

Fig. S13 : J-V plot under standard 1 sun illumination (AM 1.5 G, 100 mW/cm^2) corresponding to the initial optimization on the co-sensitization ratio with varying compositions of **RJ-C6** and **XY1b** dyes (1:1, 1.6:1, 3:1)……. 23

Table S5 : J-V parameters under standard 1 sun illumination (AM 1.5 G, 100 mW/cm^2) corresponding to the initial optimization on the co-sensitization ratio with varying compositions of **RJ-C6** and **XY1b** dyes (1:1, 1.6:1, 3:1)……. 23

Fig. S14 : J-V plot under standard 1000 lux WW CFL illumination (input power – 283 µW/cm^2) of **XY1b** dye alone……. 24

Table S6 : J-V parameter under standard 1000 lux WW CFL illumination (input power – 283 µW/cm^2) of **XY1b** dye alone…… 24

Fig. S15 : Charge collection efficiency (ηcc) for **L0:XY1b**, **DN-F13:XY1b** and **RJ-C6:XY1b** co-sensitized DSCs using dual species copper (II/I) electrolyte……. 24

Fig. S16 : Electron transport time measured using transient photocurrent decay (toolbox) method for varying co-sensitization composition ratio of **RJ-C6** and **XY1b** dyes (1:1, 1.6:1, 3:1) using dual species copper (II/I) electrolyte…… 25

Fig. S17 : Electron lifetime measured using open circuit voltage decay (OCVD) for varying co-sensitization composition ratio of **RJ-C6** and **XY1b** dyes (1:1, 1.6:1, 3:1) using dual species copper (II/I) electrolyte……... 25

Fig. S18 : Diffusion coefficient (Dn) for varying co-sensitization composition ratio of **RJ-C6** and **XY1b** dyes (1:1, 1.6:1, 3:1) using dual species copper (II/I) electrolyte…… …….. 26

Fig. S19 : Charge collection efficiency (ηcc) for varying co-sensitization composition ratio of **RJ-C6** and **XY1b** (1:1, 1.6:1, 3:1) using dual species copper (II/I) electrolyte…… …….. 26

Fig. S20 : 27

EIS spectra under dark condition (voltage ~ V_{oc}) for **L0:XY1b, DN-F13:XY1b** and **RJ-C6:XY1b** co-sensitized DSCs using dual species copper (II/I) electrolyte…… …….

Fig. S21 : IPCE response of **RJ-C6:XY1b** (ratio)co-senstized device and emission spectra of WW CFL (1000 lux) illumination……. 27

Fig. S22 : Accelerated device stability for 800 hours under continuous LED light soaking at 80% relative humidity for **RJ-C6:XY1b** (1:1) co-sensitized devices using dual species copper (II/I) electrolyte…….. 27

	Fig. S23	Post-mortem analysis of **RJ-C6:XY1b** co-sensitized devices after 800 hrs stability test under continuous LED light soaking at 80% relative humidity – (a) *in-situ* IPCE profile and (b) *ex-situ* EIS under dark condition (voltage ~ V_{oc})……	28
	Fig. S24 :	The J-V plots obtained under warm white CFL illumination intensities (ranging from 100 lux to 6000 lux: 100, 200, 500, 700, 1000, 2000, 3000, 4000, 5000, 6000 lux) for **RJ-C6:XY1b** co-sensitized devices with dual species copper (II/I) electrolyte…….	29
	Table S7 :	Tabulated J-V parameters obtained under warm white CFL illumination intensities (ranging from 100 lux to 6000 lux: 100, 200, 500, 700, 1000, 2000, 3000, 4000, 5000, 6000 lux) for **RJ-C6:XY1b** co-sensitized devices with dual species copper (II/I) electrolyte…….	29
	Table S8 :	Comparison of the best photovoltaic results obtained using triphenylamine based co-sensitized dyes and dual species ($[Cu(dmp)_2]^+$/ $[Cu(dmp)_2Cl]^+$) electrolyte from the present work with the best reported literature reports using co-sensitized dyes under standard 1000 lux CFL……	30
	Table S9 :	Comparison of the highest photovoltaic results obtained in the present study under 6000 Lux with the highest reported efficiency in literature.……	30
	Fig. S25: :	Temperature sensor/clock (ACETEQ DC-2) powered using a 2 serially interconnected DSCs (effective active area of 0.64 cm^2) fabricated using **RJ-C6**:**XY1b** co-sensitized dye combination and dual species $[Cu(II)(dmp)_2Cl]^+$/$[Cu(I)(dmp)_2]^+$(dmp-2,9-dimethyl-1,10-phenanthroline) under 1000 lux indoor WW CFL illumination……...	31
Section-VII	**Reference**……		31

Section-I. Materials

All chemicals were of the best grade commercially available (resorcinol was purchased from Spectrochem chemicals and triphenylamine was received from Merck) and were used without further purification. All solvents were purified according to the standard procedures; dry solvents were obtained according to the literature methods and stored over molecular sieves. Analytical thin-layer

chromatography was performed on polyester sheets pre-coated with silica gel containing fluorescent indicator (POLYGRAMSIL G/UV254). Gravity column chromatography was performed using silica gel and mixtures of ethyl acetate/hexanes for elution. NMR spectra were recorded with Bruker AMX-500 (500 MHz for ^{1}H NMR, 125 MHz for $^{13}C\{^{1}H\}$ NMR) instruments. All spectra were measured at 300 K, unless otherwise specified. The chemical shifts δ are given in ppm and referenced to the external standard TMS or internal solvent standard. ^{1}H NMR coupling constants (*J*) are reported in Hertz (Hz) and multiplicities are indicated as follows s (singlet), d (doublet), t (triplet), q (quartet), m (multiplet), dd (doublet of doublets). Mass spectra were performed with a ThermoFinnigan MAT95XL, a ThermoFisher Scientific LTQ Orbitrap Velos, and an Agilent 6890 gas chromatograph with JMS-T100GC spectrometer or with a ESI/ HRMS at 60,000 resolution using ThermoScientificExactive mass spectrometer with orbitrap analyzer. Florine doped tin oxide (FTO) was used as the conductive substrates (working electrode - TEC 15 Ω/cm^2, GreatCell Solar, Australia and counter electrode - TEC 7 Ω/cm^2, GreatCell Solar, Australia) for fabricating the dye sensitized solar cells. TiO_2 pastes (18-NRT, for mesoporous transparent layer and 18 NR-AO for scattering layer) were purchased from Greatcell Solar, Australia.The dyes L0, DN-F13 and XY1b were purchased from Dyenamo AB, Sweden.The dual species copper electrolyte was synthesised based on literature.[1]

Section-II. Experimental procedure for the synthesis of RJ-C6 dye

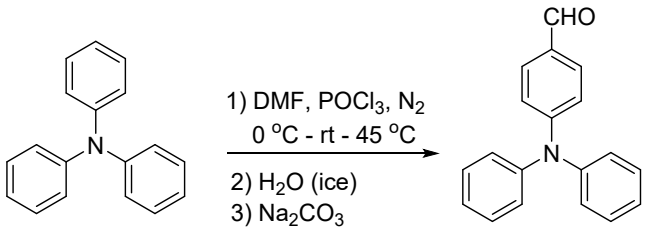

1 **2** (78%)

Synthesis of 4-(diphenylamino)benzaldehyde (2): Triphenylamine **1** (4.0 g, 16 mmol, 1.0 eq.) was dissolved in dry DMF (17.8 mL) under argon in a round bottom flask and the solution was cooled at 0°C with stirring. Phosphoryl chloride (7.6 mL, 82 mmol, 5.13 eq.) was added slowly to the mixture and stirring was continued for 30 min at 0 °C, then the reaction mixture was warmed to rt and allowed to stir for an hour. The mixture was then warmed to 45 °C and stirred for 2 more hours under argon. After the completion of the reaction as indicated by the TLC, the reaction mixture was poured into ice water and neutralized slowly with sodium hydroxide. After sedimentation and filtration, the precipitate was dried to afford **2** (3.41 g, 78%) as a light yellow solid. ^{1}H NMR ,^{13}C NMR and HRMS were in accordance with the literature.[2]

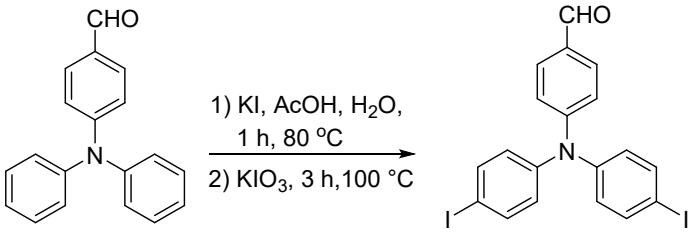

2 **3** (93%)

Synthesis of 4-(bis(4 iodophenyl)amino)benzaldehyde (3): Added 100 mL of acetic acid, 10 mL of H_2O, compound **2** (2.0 g, 7.3 mmol, 1.0 eq.), and KI (1.8 g, 10.8 mmol, 1.5 eq.) into a 250 mL three-necked flask with stirring. Warmed to 80 °C, then KIO_3 (1.7 g, 7.9 mmol, 1.1 eq.) was added and stirring was continued at 100 °C for 6 h. After the completion of the reaction as indicated by TLC, the reaction mixture was poured into water and filtered. After filtration, the precipitate was washed with distilled water repeatedly and dried, to afford **3** (3.6 g, 93%) as a yellow solid. ^{1}H NMR ,^{13}C NMR and HRMS were in accordance with the literature.[2]

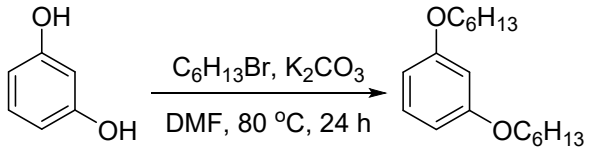

4 **5** (70%)

Synthesis of 1,3-bis(hexyloxy)benzene (5): Resorcinol **4** (1.10 g, 1.0 eq.), 1-bromohexane (2.7 mL, 3.43 g, 2.5 eq.) and potassium carbonate (5.53 g, 4.0 eq.) was added into 10 mL DMF and stirred at 80 °C for 9 h. After the completion of the reaction as indicated from TLC, the reaction mixture was concentrated under vacuum and then partitioned between water and dichloromethane. The organic layer was separated, and the aqueous layer was extracted with dichloromethane. The combined organic layers were dried over anhydrous sodium sulfate, filtered, and evaporated. The residue was then subjected to column chromatography using hexane to yield **5** as a slightly colored oil (1.94 g, 70%).^{1}H NMR ,^{13}C NMR and HRMS were in accordance with literature.[3]

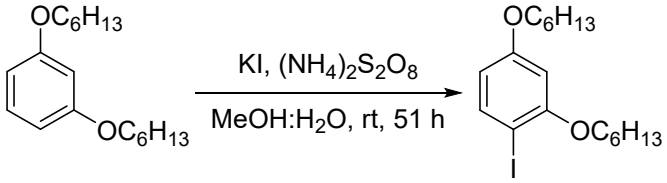

5 **6** (85%)

Synthesis of 2,4-bis(hexyloxy)-1-iodobenzene (6): The reaction was performed according to literature with slight modifications.[4] 1,3-bishexyloxybenzene **5** (474 mg, 1.0 eq.) and potassium iodide (235 mg, 1.0 eq.) and ammonium peroxodisulfate (807 mg, 2.5 eq.) in MeOH/water mixture(5 mL, 3:1) was stirred at room temperature for 51 h. After cooling, the reaction mixture was quenched with the saturated solution of sodium thiosulphate and the product was then extracted with ethyl acetate (2 × 10 ml) and washed with brine solution (2 × 10 mL), and purified using column chromatography to obtain **6** (652 mg, 85%). HRMS (ESI) m/z: $(M + H)^+$ calculated for $C_{18}H_{30}IO_2$ is 405.1290; found:405.1269; ^{1}H NMR (500 MHz, $CDCl_3$) δ 7.59 (d, *J* = 8.6 Hz, 1H), 6.40 (d, *J* = 2.5 Hz, 1H), 6.29 (dd, *J* = 8.6, 2.5 Hz, 1H), 3.97 (t, *J* = 6.4 Hz, 2H), 3.92 (t, *J* = 6.6 Hz, 2H), 1.83 (dd, *J* = 14.2, 7.3 Hz, 2H), 1.75 (dd, *J* = 14.8, 6.9 Hz, 2H), 1.55 – 1.49 (m, 2H), 1.47 – 1.40 (m, 2H), 1.37 – 1.31 (m, 8H), 0.91 (dt, J = 6.7, 3.3 Hz, 6H) ppm. ^{13}C{^{1}H} NMR (125 MHz, $CDCl_3$) δ 160.8, 158.4, 138.9, 107.6, 100.6, 77.3, 77.0, 76.8, 75.3, 69.1, 68.3, 31.6, 31.5, 29.2, 29.0, 25.8, 25.7, 22.6, 14.1 ppm.

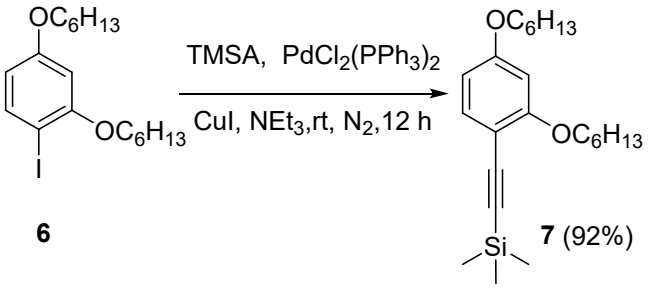

6 **7** (92%)

Synthesis of ((2,4-bis(hexyloxy)phenyl)ethynyl)trimethylsilane (7): Iododerivative **6** (420 mg, 1.0 eq.) and trimethylsilyl acetylene (122 mg, 1.2 eq) were stirred in the presence of $PdCl_2(PPh_3)_2$ (73 mg, 10 mol %) and CuI (20 mg, 10 mol %) in triethylamine (2 mL) at room temperature for 12 h under nitrogen atmosphere. After the completion of the reaction as indicated from TLC, the volatile materials were removed under reduced pressure and the oily residue was dissolved into DCM (50 mL), washed with aqueous NH_3 (10 mL × 3), and the organic layer was dried over anhydrous $MgSO_4$. The crude material was purified by column chromatography on silica gel using 2 % EtOAc/Hexane as eluent to give **7** as a highly viscous brown liquid (359 mg, 92%). HRMS (ESI) m/z: $(M + Na)^+$ calculated for $C_{23}H_{38}NaO_2Si$ is 397.2539; found: 397.2556.^{1}H NMR (500 MHz, $CDCl_3$) δ 7.31 (d, *J* = 8.7 Hz, 1H), 6.38 (d, *J* = 7.0 Hz, 2H), 3.97 – 3.91 (m, 4H), 1.83 – 1.79 (m, 2H), 1.78 – 1.74 (m, 2H), 1.54 – 1.50 (m, 2H), 1.44 (d, *J* = 7.0 Hz, 2H), 1.34 (s, 8H), 0.90 (s, 6H), 0.24 (s, 9H) ppm. $^{13}C\{^1H\}$ NMR (125 MHz, $CDCl_3$) δ 161.4, 160.7, 134.2, 105.1, 104.9, 101.5, 99.6, 96.2, 77.1, 76.9, 76.6, 68.4, 67.9, 31.5, 31.4, 29.0, 29.0, 25.6, 25. 6, 22.5, 22.5, 13.9, 13.9, 0.9 ppm.

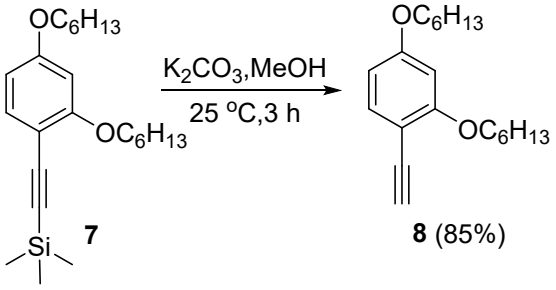

7 **8** (85%)

Synthesis of 1-ethynyl-2,4-bis(hexyloxy)benzene (8): A mixture of **7** (540 mg, 1.0 eq.), and anhydrous potassium carbonate (18 mg, 0.09 eq.) in anhydrous MeOH (1.5 mL) was stirred at room temperature for 3 h. The solvent was evaporated under reduced pressure, and the residue was mixed with 2 mL of aqueous sodium bicarbonate and extracted with Et_2O (3 × 10 mL). The combined organic fractions were dried over $MgSO_4$ and concentrated. The residue was purified by silica gel column chromatography using 2 % EtOAc/Hexane as eluent to obtain **8** highly viscous brown liquid (435 mg, 85%). HRMS (ESI) m/z: (M + H) calculated

for $C_{20}H_{31}O_2$ is 303.2324;found: 303.2318. ^{1}H NMR (500 MHz, $CDCl_3$) δ 7.34 (d, *J* = 9.1 Hz, 1H), 6.41 (d, *J* = 6.6 Hz, 2H), 4.00 (t, *J* = 6.7 Hz, 2H), 3.94 (t, *J* = 6.6 Hz, 2H), 3.17 (s, 1H), 1.83 (dd, *J* = 14.3, 7.2 Hz, 2H), 1.76 (dd, *J* = 14.7, 6.9 Hz, 2H), 1.50 – 1.44 (m, 4H), 1.36 – 1.33 (m, 7H), 0.90 (dd, *J* = 6.6, 4.4 Hz, 5H) ppm. ^{13}C{^{1}H} NMR (125 MHz, CDCl3) δ 161.5, 161.3, 160.9, 134.8, 105.4, 103.9, 99.9, 79.4, 77.3, 77.0, 76.8, 68. 8, 68.2, 31.6, 31.5, 29.2, 28.9, 25.7, 25.6, 22.6, 14.0, 14.0 ppm.

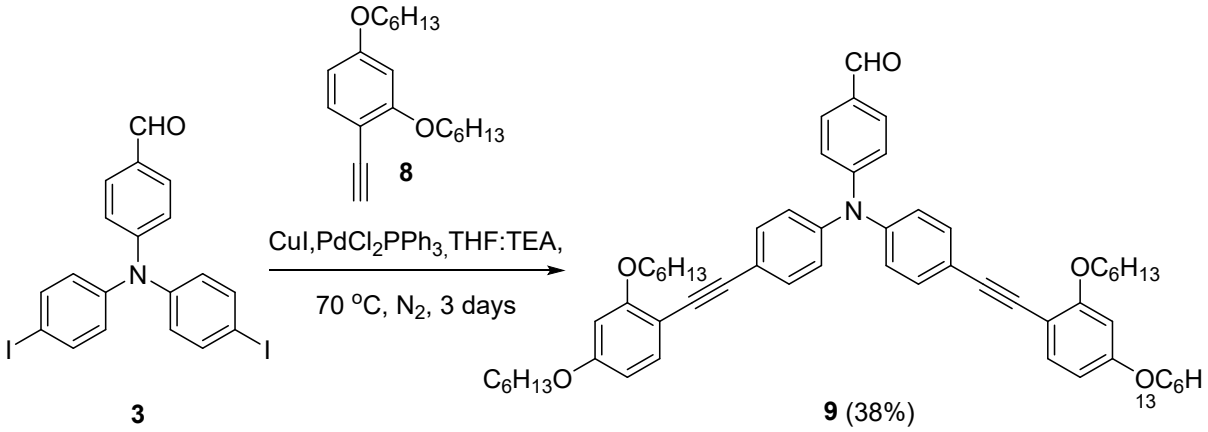

3 **9** (38%)

Synthesis of 4-(bis(4-((2,4-bis(hexyloxy)phenyl)ethynyl)phenyl)amino)benzaldehyde (9):

3 (343 mg, 1.0 eq.), **8** (594 mg, 3.0 eq.), dichlorobis(triphenylphosphine)palladium (II) (46 mg, 10 mol %) and copper(I) iodide (12 mg, 10 mol %) were taken in a nitrogen purged schlenk tube. 6 mL of anhydrous THF:TEA mixture (1:1) was taken in a in a previously degassed argon purged conical flask. The mixture was added to schlenk tube under Nitrogen flow, and was stirred and heated at 70 °C for 3 days. After the completion of the reaction as indicated from the TLC, the reaction mixture was concentrated to give a residue which was chromatographed over silica gel (230–400 mesh) and product **9** was extracted as a brownish -green viscous liquid using 5% EtOAc/Hexane mixture (217 mg, 38%). HRMS (ESI) m/z: $(M + Na)^+$ calculated for $C_{59}H_{72}NNaO_5$ is 896.5230;found: 896.4813. ^{1}H NMR (500 MHz, $CDCl_3$) δ 9.85 (s, 1H), 7.72 (d, *J* = 8.6 Hz, 2H), 7.46 (d, *J* = 8 Hz, 4H), 7.37 (d, *J* = 9.0 Hz, 2H), 7.11 (t, *J* = 7.1 Hz, 6H), 6.45 (d, *J* = 6.7 Hz, 4H), 4.02 (t, *J* = 6.4 Hz, 4H), 3.96 (t, *J* = 6.5 Hz, 4H), 1.88 – 1.82 (m, 4H), 1.79 (d, *J* = 7.1 Hz, 4H), 1.58 – 1.52 (m, 4H), 1.50 – 1.44 (m, 4H), 1.39 – 1.33 (m, 15H), 0.92 – 0.86 (m, 12H) ppm. ^{13}C{^{1}H} NMR (125 MHz, $CDCl_3$) δ 189.4, 159.9, 159.7, 151.5, 144.2, 132.8, 131.7, 130.3, 124.4, 119.9, 119.6, 104.5, 104.1, 98.9, 90.4, 85.7, 76.3, 76.0, 75.8, 67.7, 67.2, 30.6, 30.6, 28.7, 28.3, 28.1, 24.7, 21.6, 21.7, 13.0.

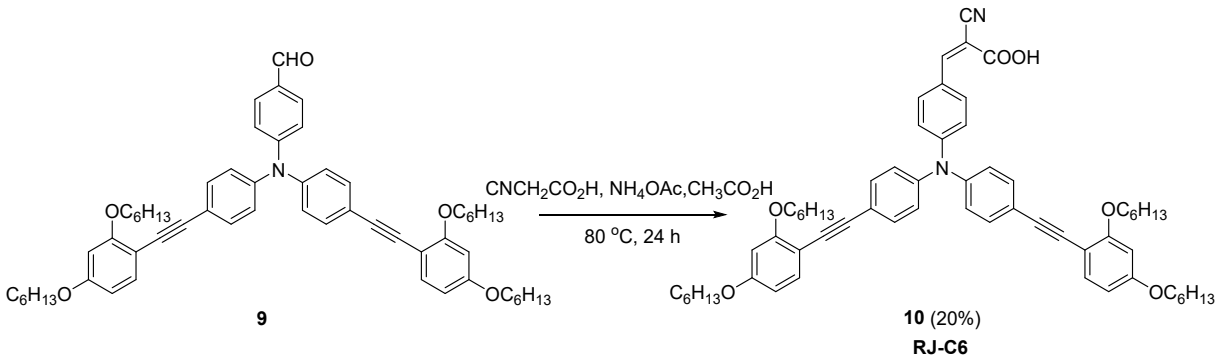

Synthesis of 3-(4-(bis(4-((2,4-bis(hexyloxy)phenyl)ethynyl)phenyl)amino)phenyl)-2-cyanoacrylic acid (RJ-C6): A mixture of aldehyde **9** (313 mg, 1.0 eq.), cyanoacetic acid (45.6 mg, 1.5 eq.), and ammonium acetate (53.8 mg, 1.95 eq.) in glacial acetic acid (5 mL) was stirred at 80 °C for 24 h. After complete consumption of aldehyde, the reaction mixture was cooled to room temperature and it was quenched by adding ice-cold water. The aqueos layer was extracted thrice using dichloromethane and the organic layer was dried over sodium sulphate, and evaporated to yield a reddish sticky crude. It was then purified using column chromatography (30% EA/Hexane) to yield **RJ-C6** as a dark red solid (67 mg, 20%). HRMS (ESI) m/z: $(M + Na)^+$ calculated for $C_{62}H_{72}N_2NaO_6$ is 963.5288; found: 963.5225. ^{1}H NMR (500 MHz, $CDCl_3$) δ 8.14 (s, 1H), 7.91 (d, *J* = 8.6 Hz, 2H), 7.47 (d, *J* = 8.2 Hz, 4H), 7.37 (d, *J* = 8.2 Hz, 2H), 7.11 (d, *J* = 8.2 Hz, 4H), 7.07 (d, *J* = 8.6 Hz, 2H), 6.45 (d, *J* = 7.9 Hz, 4H), 4.02 (t, *J* = 6.4 Hz, 4H), 3.96 (t, *J* = 6.5 Hz, 4H), 1.90 – 1.84 (m, 4H), 1.81 – 1.76 (m, 4H), 1.57 – 1.52 (m, 4H), 1.50 – 1.44 (m, 4H), 1.36 – 1.32 (m, 16H), 0.92 – 0.87 (m, 12H) ppm. ^{13}C{^{1}H} NMR (125 MHz, $CDCl_3$) δ 160.9, 160.8, 144.7, 133.9, 133.5, 132.8, 132.3, 132.2, 128.7, 128.6, 125.7, 121.2, 120.5, 105.5, 105.1, 99.9, 77.3, 77.1, 76.8, 68.7, 68.2, 31.6, 31.6, 29.2, 29.2, 25.7, 22.7, 22.6, 14.1 ppm.

Section-III.

Fig. S1-S10:Structural characterization of precursors and RJ-C6 dye (^{1}H NMR, ^{13}C NMR)

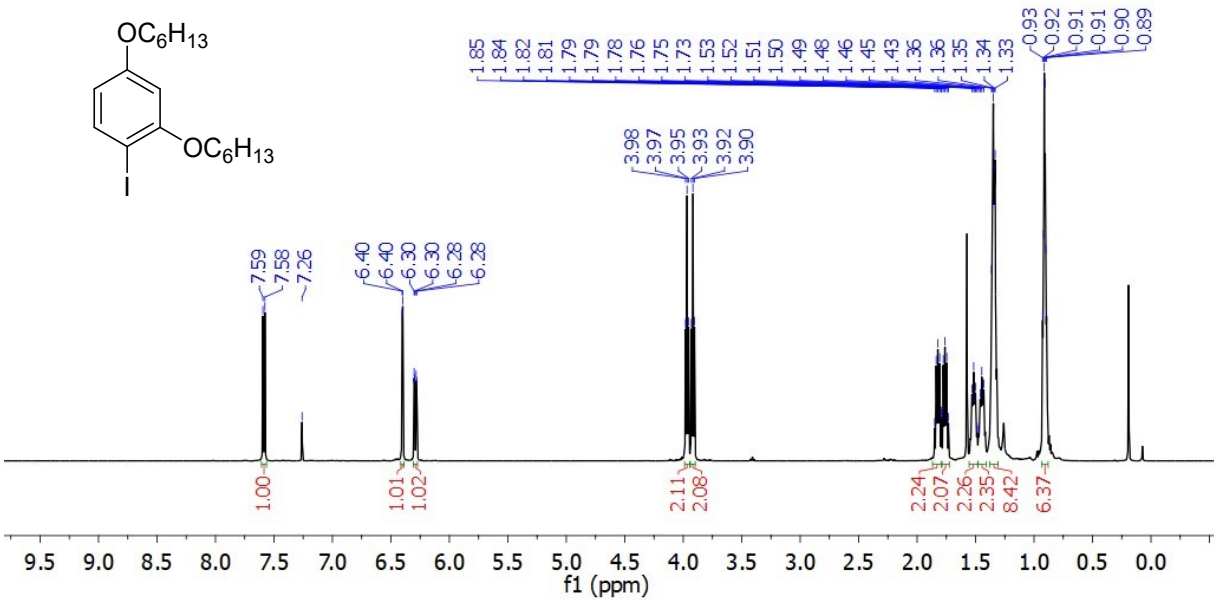

Fig. S1: ^{1}H NMR spectrum of compound **6**

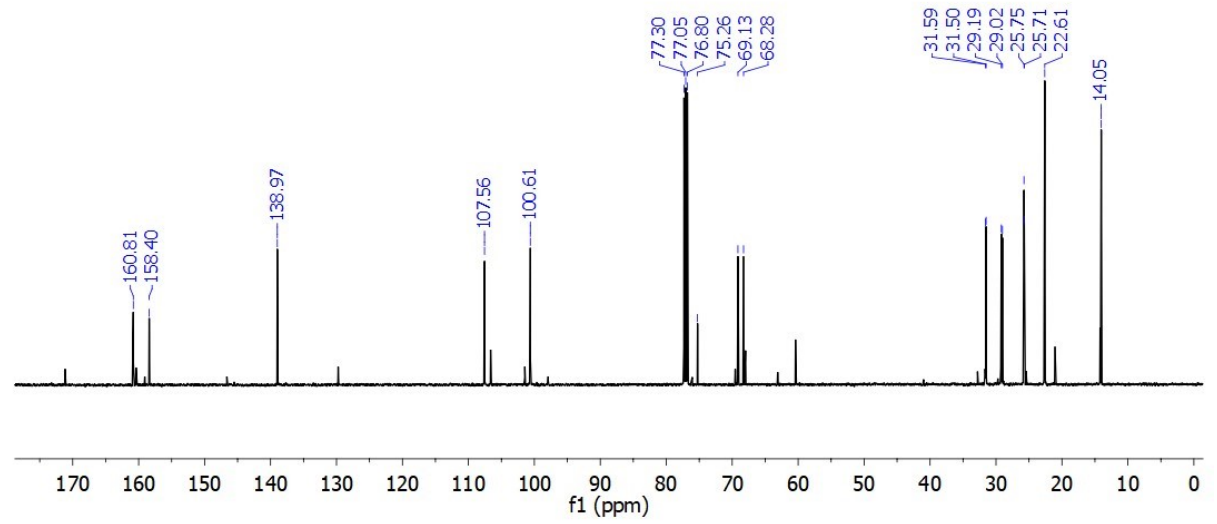

Fig. S2: ^{13}C NMR spectrum of compound **6**.

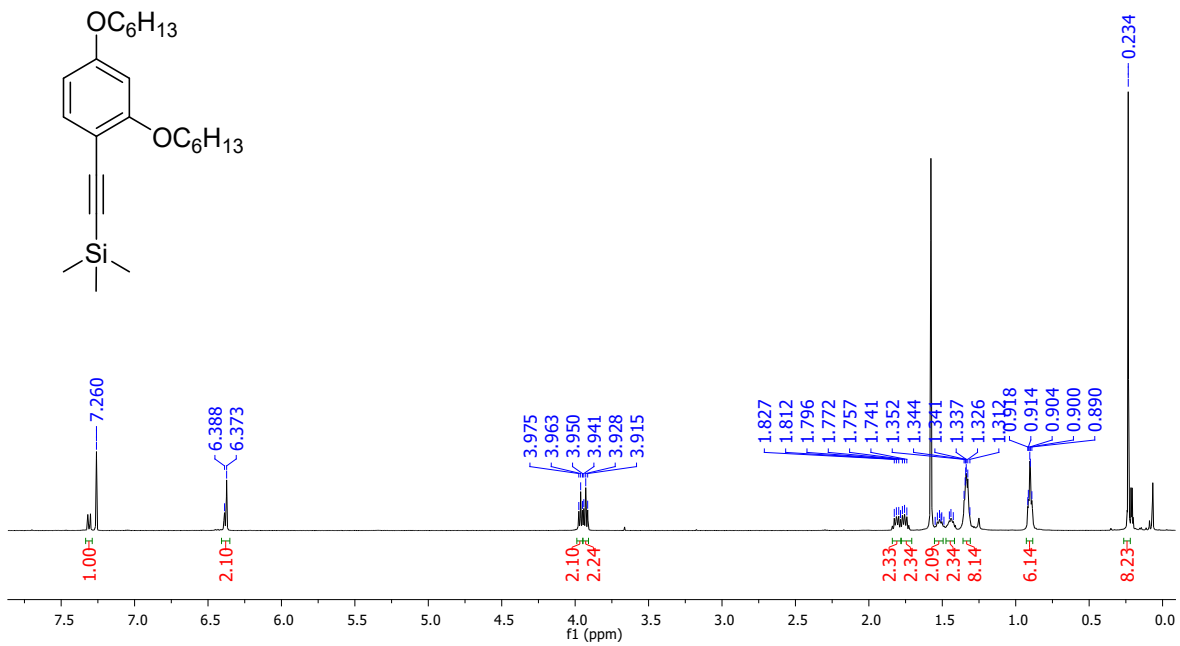

Fig. S3: ^{1}H NMR spectrum of compound **7**

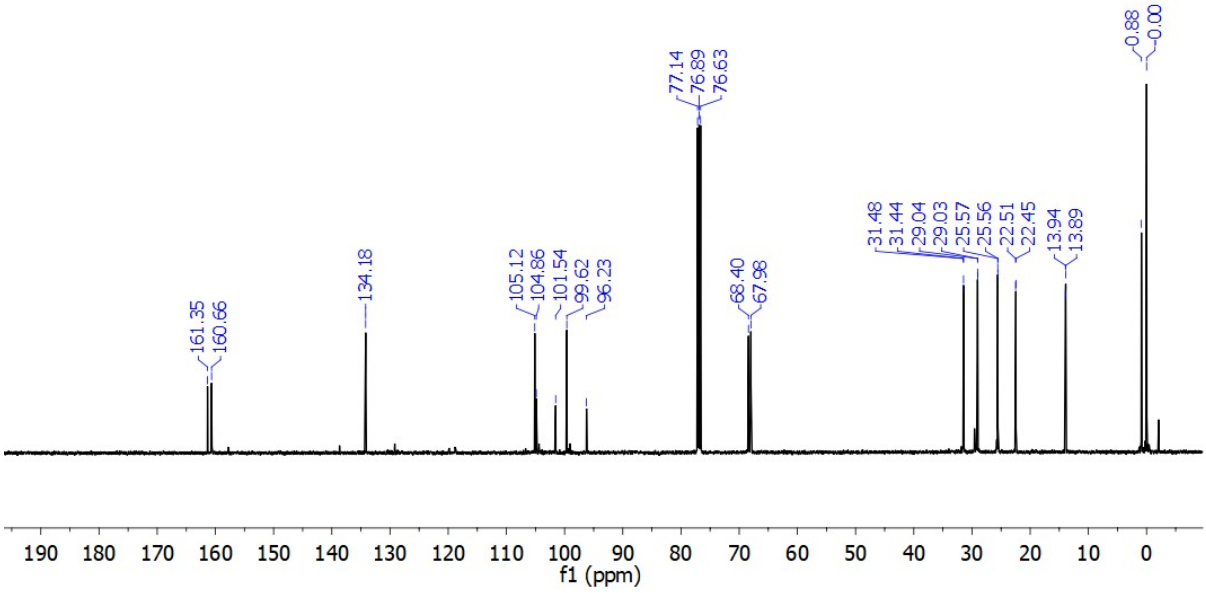

Fig. S4: ^{13}C NMR spectrum of compound **7**

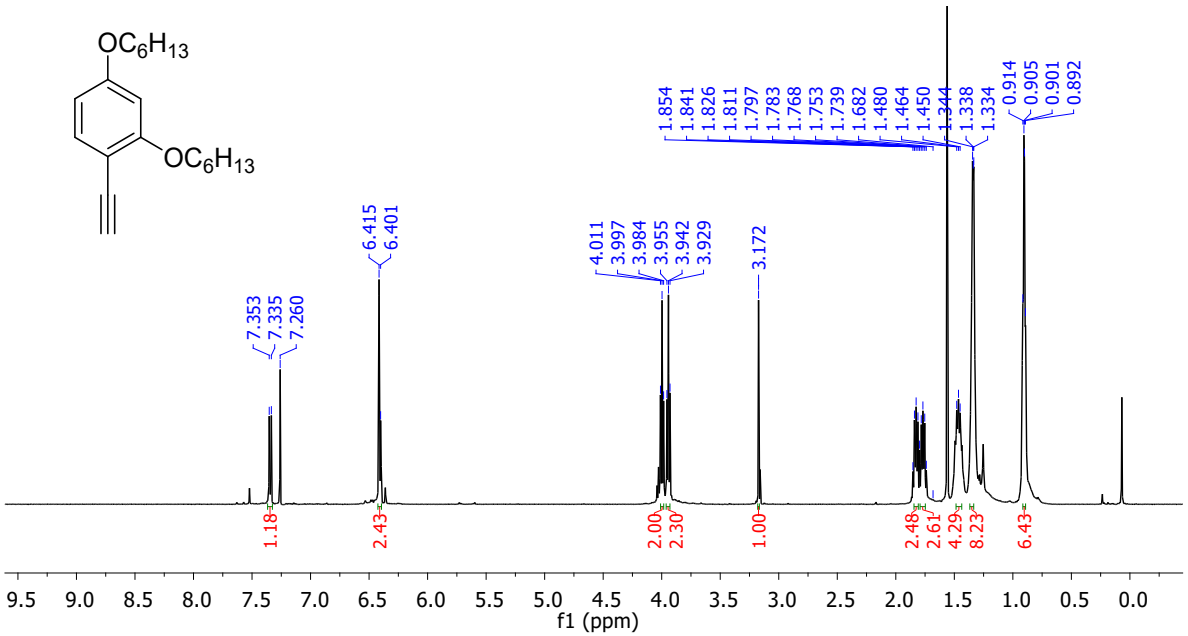

Fig. S5: ^{1}H NMR spectrum of compound **8**

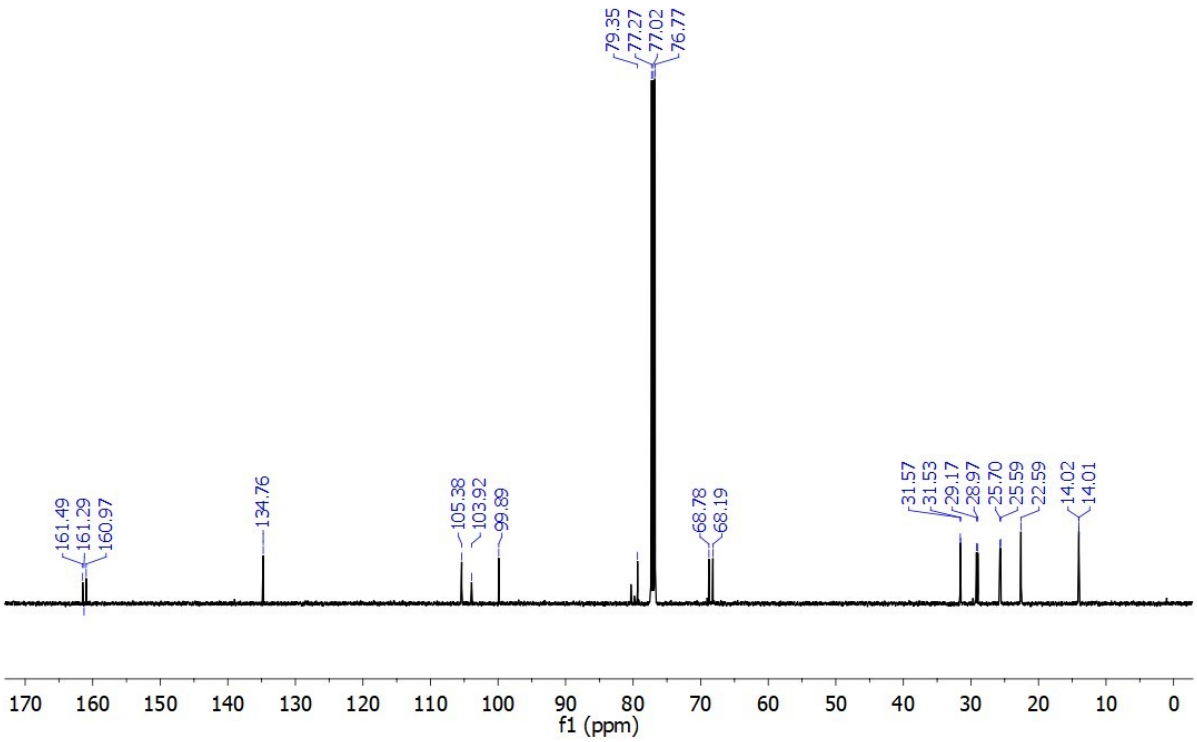

Fig. S6: ^{13}C NMR spectrum of compound **8**

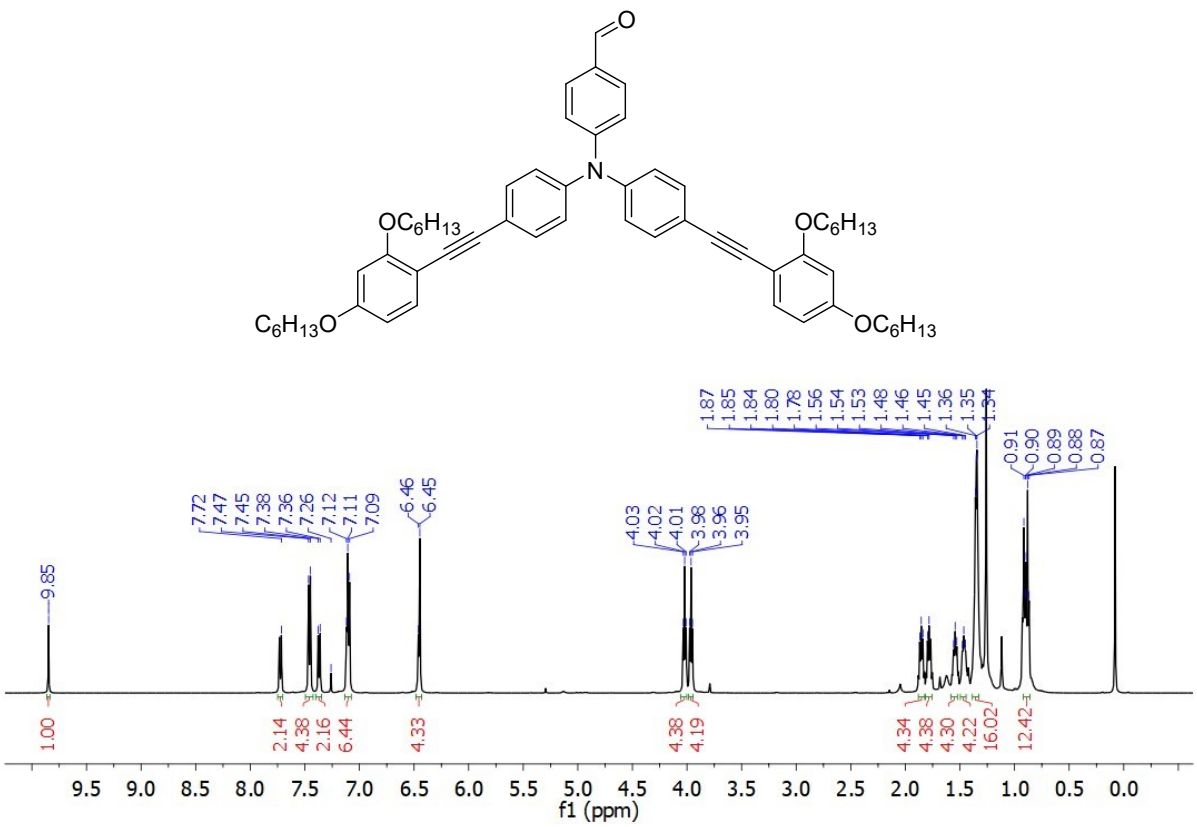

Fig. S7: ^{1}H NMR spectrum of compound **9**.

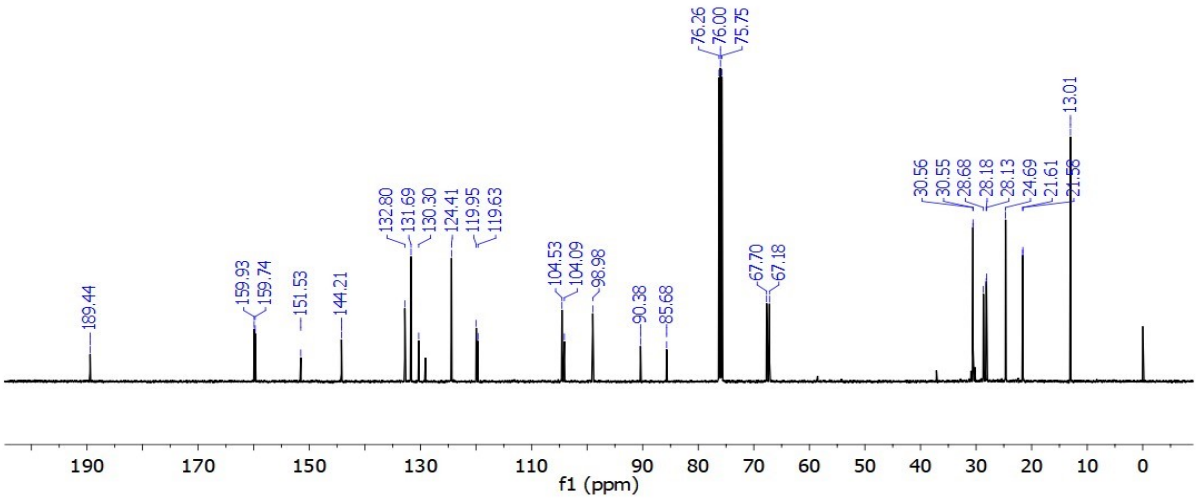

Fig. S8: ^{13}C NMR spectrum of compound **9**.

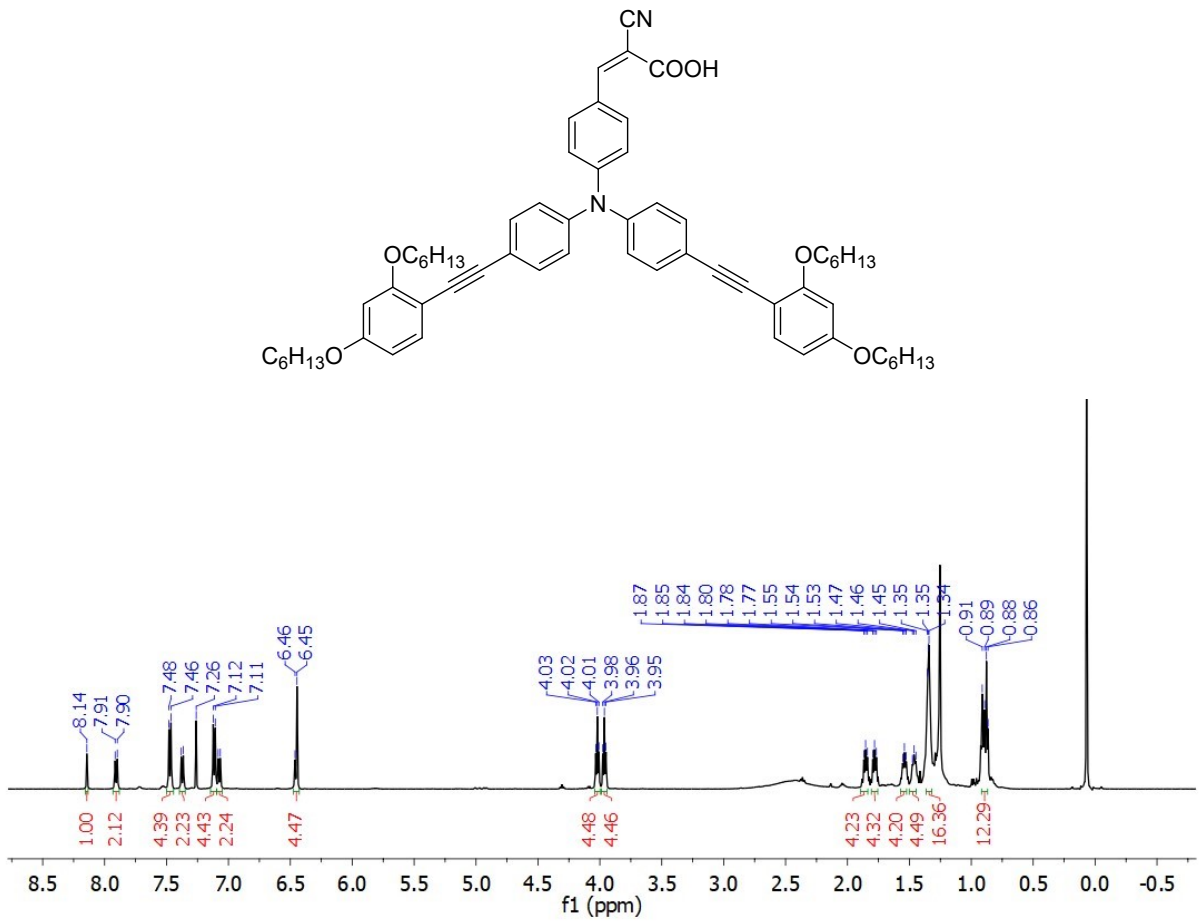

Fig. S9: ^{1}H NMR spectrum of compound **RJ-C6**

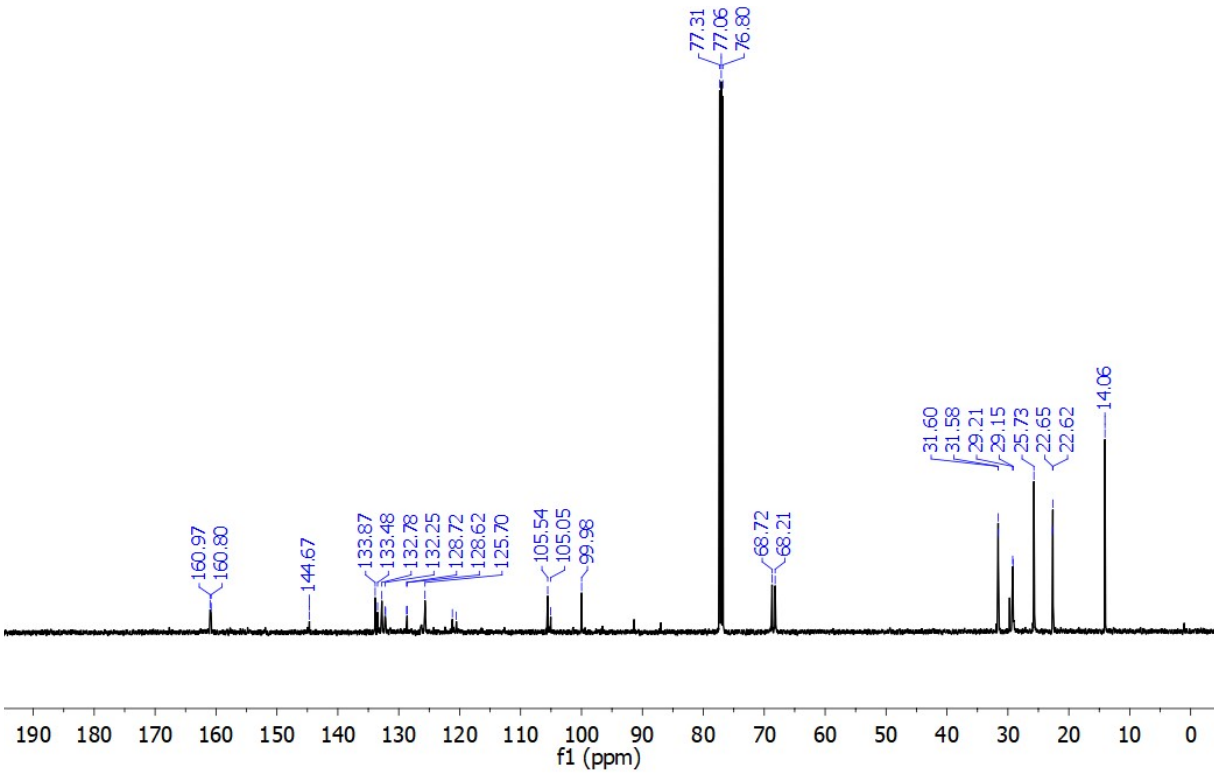

Fig. S10: ^{13}C NMR spectrum of compound **RJ-C6**

Section-IV. Dye loading

UV-Visible spectrometer (Jaz spectrometer, Ocean Optics) was used to carry out the dye loading studies as described below. The dye solution (same concentration as used in device) is divided into two equal portions (solution 1 and solution 2). The photoanode (FTO coated with the mesoporous TiO_2), whose dye loading is to be obtained, is immersed in solution 2. After 16 hrs of dye soaking, solution 2 is retrieved. The photoanode is then washed with 1 mL of acetonitrile to remove the weakly adsorbed dye which is also added to solution 2. To compensate for the variation in concentration, the same amount of acetonitrile is added to solution 1. Now, the UV-visible absorption spectra of both solutions are recorded and the absorbance is obtained as abs1 and abs2 for solutions 1 and 2 respectively.Finally, the amount of dye adsorbed per unit area (mol/cm^2) of the mesoporous layer is estimated using the equation:

$$dye\ loading = (abs1 - abs2)V/\boldsymbol{\varepsilon sl}$$

where V is the volume of the solution, ε is the molar extinction coefficient of the dye, s is the photoanode's active area, and l is the path length of the incident light in the solution

Section-V. Theoretical studies of the Dyes

Table S1 The dihedral angles in **L0**, **DNF-13**, and **RJ-C6**

Dihedral Angles (◦)	Dyes		
	L0	**DN-F13**	**RJ-C6**
	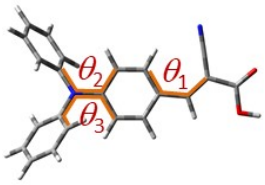	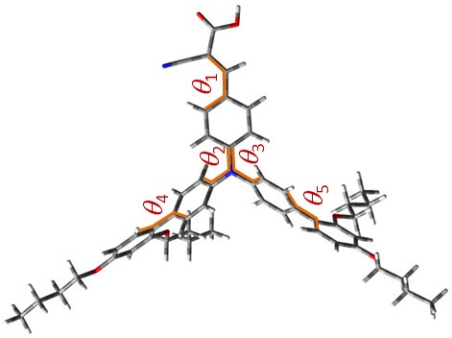	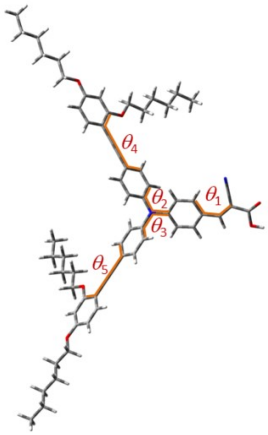
θ_1	0.42179	0.25655	0.62877
θ_2	50.28522	51.06167	48.59888
θ_3	51.00577	52.12239	50.20267
θ_4	-	44.07716	1.57434
θ_5	-	44.02002	0.68141

Fig. S11: Side view of the dyes **RJ-C6**, **DN-F13** and **L0** obtained from DFT calculations.

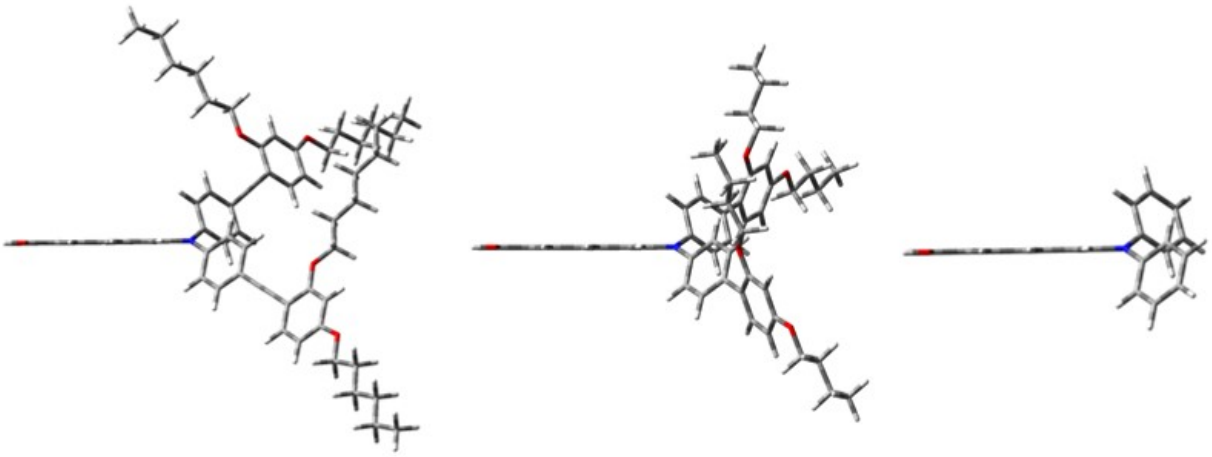

RJ-C6 **DN-F13** **L0**

Fig. S12(a-d): The length of the molecules **L0**, **DN-F13**, **RJ-C6** and **XY1b** from DFT calculations.The distances are between respective atom to atom.

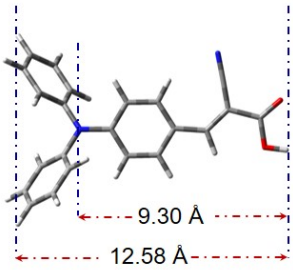

Fig. S12a: **L0**

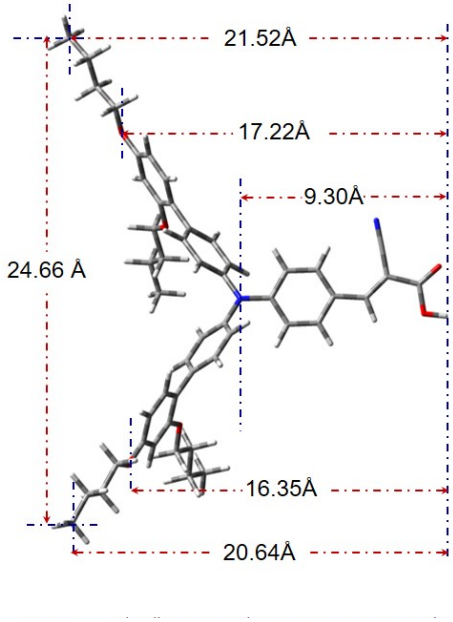

Fig. S12b: **DN-F13**

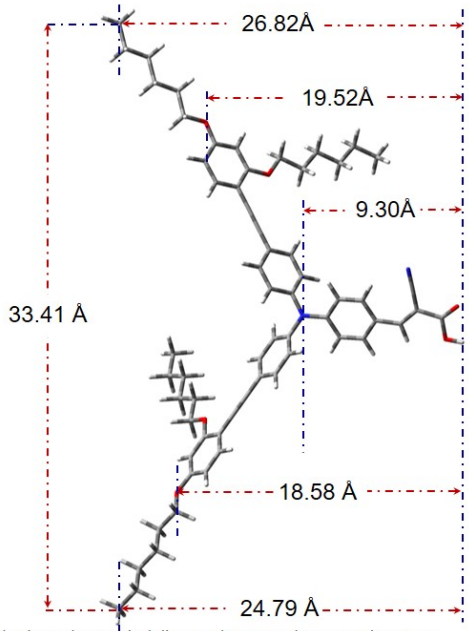

Fig. S12c: **RJ-C6**

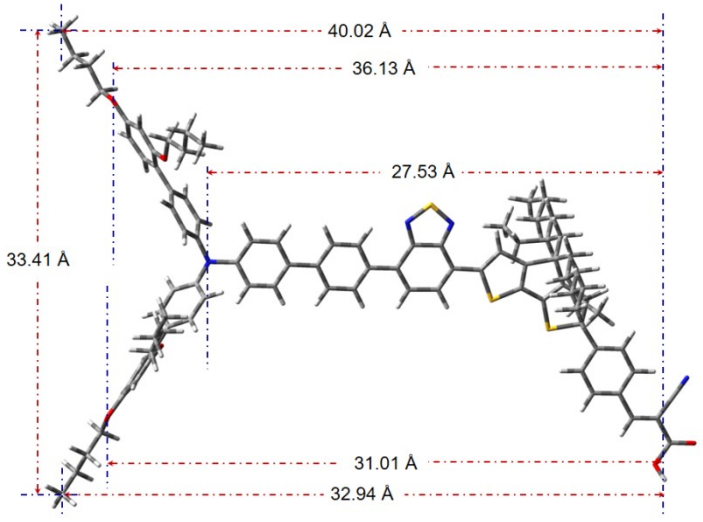

Fig. S12d: **XY1b**

Table S2: TD-DFT calculated prominent electronic transitions of **L0**.

	Chloroform			Gas Phase		
1.	89 → 90	0.70435	446.58 nm f=0.8986	89 → 90	0.70196	413.59 nm f=0.7762
2.	84 → 90 87 → 90 89 → 91	-0.12873 0.20422 0.65200	317.89 nm f=0.0221	87 → 90 89 → 91	0.13720 0.67129	320.50 nm f=0.0220
3.	86 → 90 88 → 90 89 → 93	-0.14720 0.67479 0.12024	302.35 nm f=0.1674	89 → 91 89 → 92	0.12115 0.68131	301.60 nm f=0.1214
4.	84 → 90 87 → 90 89 → 91 89 → 92	-0.17225 0.22037 -0.16762 0.61553	298.38 nm f=0.1424	86 → 90 88 → 90 89 → 93	-0.16249 0.62873 -0.25268	291.35 nm f=0.2031
5.	84 → 90 87 → 90 89 → 91 89 → 92	-0.17345 0.55310 -0.19234 -0.30223	295.07 nm f=0.0242	83 → 90 85 → 90 86 → 90 87 → 90 88 → 90 89 → 91 89 → 94 89 → 95	-0.12563 0.27733 0.16085 0.47180 0.10943 -0.14985 0.19302 0.25631	288.44 nm f=0.0178
6.	86 → 90 87 → 90 88 → 90 89 → 93 89 → 95	0.64913 -0.14129 0.12755 0.12023 -0.13485	289.36 nm f=0.1560	83 → 90	0.67808	286.71 nm f=0.0003
7.	84 → 90 86 → 90 87 → 90 89 → 93 89 → 94 89 → 95	0.54277 0.11417 0.27827 0.12537 0.24029 0.14312	284.36 nm f=0.0115	86 → 90 87 → 90 88 → 90 89 → 94 89 → 95	0.44843 -0.21473 0.12516 -0.38149 0.25118	279.89 nm f=0.0388
8.	83 → 90 83 → 96 85 → 90	0.68231 -0.10162 -0.12075	276.90 nm f=0.0014	85 → 90 87 → 90 89 → 94 89 → 95	-0.28750 0.44454 -0.40559 -0.17840	275.56 nm f=0.0022
9.	83 → 90 84 → 90 85 → 90	0.12044 0.10341 0.67858	274.26 nm f=0.0473	85 → 90 86 → 90 89 → 93 89 → 94 89 → 95	0.16525 -0.41100 0.46696 -0.12383 0.21472	273.90 nm f=0.0175
10.	89 → 93 89 → 94 89 → 95	0.24478 -0.42922 0.46899	271.34 nm f=0.0083	85 → 90 86 → 90 88 → 90 89 → 93 89 → 94 89 → 95	-0.30841 0.23762 0.20767 0.40394 0.33340 -0.10079	267.11 nm f=0.0150
11.	84 → 90 86 → 90 89 → 93 89 → 94	-0.22116 -0.11494 0.56876 0.28586	270.46 nm f=0.0084	84 → 90 85 → 90 89 → 93 89 → 95	0.34269 -0.35170 -0.11233 0.44300	261.71 nm f=0.1030
12.	84 → 90 89 → 93 89 → 94 89 → 95	-0.22583 -0.23028 0.37398 0.46471	265.26 nm f=0.0728	84 → 90 85 → 90 89 → 95	0.60976 0.20795 -0.25090	261.22 nm f=0.0042

Table S3: TD-DFT calculated prominent electronic transitions of **DN-F13**.

	$CHCl_3$			Gas Phase		
1.	209 → 210	0.70460	489.27 nm f=0.8012	209 → 210	0.70237	455.99 nm f=0.7092
2.	208 → 210	0.70555	409.48 nm f=0.0645	208 → 210	0.70497	385.88 nm f=0.0620
3.	207 → 210	0.70108	376.03 nm f=0.3259	207 → 210	0.69447	356.48 nm f=0.3152
4.	209 → 211	0.68729	338.03 nm f=0.5849	209 → 211 209 → 212	0.68615 -0.11649	338.74 nm f=0.5012
5.	206 → 210	0.70032	331.37 nm f=0.0355	209 → 211 209 → 212 209 → 213	0.12619 0.65460 0.13440	322.06 nm f=0.1400
6.	205 → 210	0.70014	328.76 nm f=0.0276	206 → 210	0.69815	316.54 nm f=0.0291
7.	203 → 210 209 → 211 209 → 212 209 → 213	0.14780 0.10012 0.65430 0.10328	321.26 nm f=0.1655	205 -> 210 209 -> 213	0.69267 -0.11445	311.43 nm f=0.0275
8.	202 → 210 204 → 210 209 → 213	-0.10819 0.62498 -0.26694	303.80 nm f=0.0898	204 → 210 205 → 210 209 → 212 209 → 213	-0.30197 0.11772 -0.12678 0.58527	298.82 nm f=0.0630
9.	202 → 210 203 → 210 204 → 210 209 → 212 209 → 213	-0.32507 0.22687 0.19048 -0.14586 0.49876	298.67 nm f=0.0758	201 → 210 203 → 210 204 → 210 209 → 213 209 → 214	0.12944 0.41586 -0.39804 -0.19424 0.27440	292.30 nm f=0.0105
10.	200 → 210 201 → 210 202 → 210 203 → 210 209 → 212 209 → 213 209 → 214	0.20225 -0.11509 0.13998 0.56399 -0.13676 -0.24095 0.12000	297.67 nm f=0.016	201 → 210 202 → 210 203 → 210 204 → 210 209 → 212 209 → 214 209 → 215	0.31074 0.40840 0.11591 0.23074 -0.13606 0.18533 0.26348	291.19 nm f=0.0121
11.	200 → 210 201 → 210 202 → 210 203 → 210 204 → 210 208 → 211 209 → 213 209 → 214	0.17056 -0.11800 -0.22486 -0.14477 -0.10336 0.52901 -0.14281 0.19809	289.26 nm f=0.1162	203 → 210 204 → 210 208 → 211 209 → 215	-0.17726 -0.17701 0.61564 0.13187	285.99 nm f=0.1454
12.	200 → 210 201 → 210 203 → 210 208 → 211 209 → 214	0.33712 -0.23985 -0.25957 -0.29827 0.34840	288.71 nm f=0.0324	199 → 210 202 → 210 203 → 210 209 → 214	0.62469 -0.14269 -0.14031 0.17996	284.48 nm f=0.0014

Table S4: TD-DFT calculated prominent electronic transitions of **RJ-C6**

	$CHCl_3$		Gas Phase	
1.	253 → 254 0.70412	524.33 nm f=0.7789	253 → 254 0.70496	499.83 nm f=0.6320
2.	252 → 254 0.70511	445.80 nm f=0.1702	252 → 254 0.70522	434.48 nm f=0.1286
3.	253 → 255 0.69726	398.93 nm f=1.4514	253 → 255 0.69793	394.56 nm f=1.3434
4.	251 → 254 0.67583 253 → 256 -0.17658	387.46 nm f=0.5481	251 → 254 0.65871 253 → 256 -0.22932	375.27 nm f=0.5872
5.	251 → 254 0.11621 252 → 255 0.32774 253 → 256 0.57920 253 → 257 0.15832	342.52 nm f=0.0039	251 → 254 0.10294 252 → 255 0.40593 253 → 256 0.47638 253 → 257 0.28495	343.05 nm f=0.0118
6.	249 → 254 0.10745 250 → 254 0.10870 251 → 254 -0.11747 252 → 255 0.57027 253 → 256 -0.19280 253 → 257 -0.27816	338.16 nm f=0.3113	252 → 255 -0.28973 253 → 256 -0.13291 253 → 257 0.60859	339.43 nm f=0.0632
7.	249 → 254 0.10992 252 → 255 0.16253 253 → 256 -0.22493 253 → 257 0.59665	335.22 nm f=0.0765	248 → 254 -0.11630 249 → 254 0.14526 250 → 254 0.22286 251 → 254 -0.19963 252 → 255 0.44401 253 → 256 -0.38016 253 → 257 0.11379	328.53 nm f=0.2498
8.	249 → 254 -0.14514 250 → 254 0.67768	327.70 nm f=0.0140	249 → 254 -0.17173 250 → 254 0.65479 252 → 255 -0.11555 253 → 256 0.12490	319.02 nm f=0.0159
9.	249 → 254 0.66953 250 → 254 0.11142 252 → 255 -0.11496 253 → 256 0.13610	324.42 nm f=0.0056	249 → 254 0.66033 250 → 254 0.12528 252 → 255 -0.11821 253 → 256 0.12889	313.67 nm f=0.0048
10.	251 → 255 0.52164 252 → 256 0.44697	312.57 nm f=0.4673	251 → 255 0.61313 252 → 256 0.29390	310.34 nm f=0.3620
11.	251 → 255 -0.45003 252 → 256 0.52653	306.44 nm f=0.0879	251 → 255 -0.30415 252 → 256 0.62253	306.64 nm f=0.2021
12.	246 → 254 -0.26302 248 → 254 0.48574 252 → 257 -0.25433 253 → 258 -0.12291 253 → 259 0.29233	300.24 nm f=0.0546	246 → 254 0.17720 248 → 254 -0.15031 252 → 257 0.43972 253 → 258 -0.34763 253 → 259 -0.29936	300.15 nm f=0.0233

Section-VI. Device fabrication and characterization

Device fabrication involves systematic protocol as described in our previous works[1,5,6].The entire device fabrication was done using the semi-automatic DSC fabrication facility at CSIR-NIIST. FTO substrates (TEC 15 Ω/cm^2, GreatCell Solar, Australia) for the working electrodes were cleaned in detergent solution, distilled water, acetone, and isopropanol, followed by annealeing at 500 °C using a pre-programed ramp heating, 325 °C for 15 min, 375 °C for 15 min, 450 °C for 15 min, and 500 °C for 30 min. The annealed FTO substrates were UV-Ozone treated before immersing in aqueous 53 mM $TiCl_4$ solution at 70 °C for 30 min for the deposition of TiO_2 pre-blocking layers. The transparent TiO_2 layer (18-NRT, GreatCell Solar, Australia)[1,7,8] was deposited on FTO glass using screen printing technique followed by annealing at 100 °C. Further, the scattering layer (18 NR-AO, GreatCell Solar, Australia) was also deposited via screen printing, thereby producing an effective TiO_2 layer thickness of ~ 8 µm (measured using a profilometer, Bruker Dektak XT). The electrodes were again annealed using the same program mentioned earlier. For the deposition of the post blocking layer, the annealed electrodes were immersed in aqueous 53 mM $TiCl_4$ solution for 30 min at 70 °C and further heat-treated at 500 °C. The electrodes were then immersed in **L0** (Dyenamo AB, Sweden), **DN-F13** (Dyenamo AB, Sweden) and **RJ-C6** dye solutions (0.2 mM) for dye alone and for the co-sensitized devices using **XY1b** obtained from Dyenamo AB, Sweden in ratio **L0:XY1b** (0.1 mM each), **DN-F13:XY1b** (0.1 mM each) and **RJ-C6:XY1b** (0.1 mM each) in 1:1 mixture of acetonitrile and *tert*-butanol and kept at room temperature for 16 h for effective dye loading. Pre-drilled counter electrodes (TEC 7 Ω/cm^2, GreatCell Solar, Australia) were cleaned using the same protocol for the photoanode. The catalytic property of the counter electrode was enhanced via electrochemical deposition of EDOT, resulting in the formation of PEDOT (electrodeposition is done in galvanostatic mode using Metrohm Autolab, PGSTAT 302N).[9] The electrodes were then assembled using UV curable epoxy.The space between the electrodes was filled with liquid dual species $[Cu(II)(dmp)_2Cl]^+/[Cu(I)(dmp)_2]^+$(dmp-2,9-dimethyl-1,10-phenanthroline) electrolyte using the standard composition of 0.2 M bis-(2,9-dimethyl-1,10-phenanthroline)copper(I)bis(trifluoromethanesulfonyl)imide, 0.04 M bis-(2,9-dimethyl-1,10-phenanthroline)copper(II)bis(trifluoromethanesulfonyl)imide chloride, 0.1 M Lithium bis(trifluoromethanesulfonyl)imide (LiTFSI) and 0.6 M NMBI in acetonitrile. The holes were then sealed to avoid electrolyte leakages using cover glass.

Photocurrent density voltage (*J*–*V*) characterization of the fabricated solar cells was done under AM 1.5G simulated light (100 $mWcm^{-2}$) using a class AAA solar simulator (Oriel 3A, Model PVIV- 94023A, Newport) coupled with Keithley 2440 source meter. One batch consist of 12 devices for each condition and was repeated three times to calculate the standard error deviation and reproducibility. The error for the photovoltaic parameters were calculated by taking the obtained average values of individual parameters and then calculating the standard deviation as average error value. A 250 W Xenon lamp coupled with a monochromator setup (Newport) was deployed for the incident photon-to-current conversion efficiency (IPCE) measurements of the devices. *J*–*V* measurement under indoor light conditions was carried out using a custom-made setup with a warm white-fluorescent lamp/light source (Osram WWCFL, 100-1000 lux)[1,5,6]. Advanced interfacial device characterizations like charge extraction (CE) and open-circuit voltage decay (OCVD) were performed using Autolab-PGSTAT 302N (Metrohm) electrochemical workstation. OCVD measurements were performed using white LED as the illumination source, measuring the voltage decay of the deacy under open circuit conditions to determine the electron lifetime within the meso-TiO_2 layer. Similarly, for charge extraction, the devices in open circuit condition is illuminated for a few seconds and the illumination is stopped simultaneously short-circuiting to extract the charge. Transient photovoltage and photocurrent decay measurements were performed using toolbox (Dyenamo AB, Sweden), with light from a white LED as bias and modulation of less than 10% of the steady-state value. For transient photovoltage decay, the device is initially open circuited and simultaneously illuminated till it reaches to a steady voltage (V_{oc}). A square wave light perturbation is further superimposed and the voltage response of the solar cell is monitored. While for transient photovoltage decay, device is short circuited and illuminated till it reaches to the steady state J_{sc}. A square wave light perturbation is then superimposed with the steady illumination and the current response of the solar cell is further monitored.

Fig. S13: *J-V* plot under standard 1 sun illumination (AM 1.5 G, 100 mW/cm^2) corresponding to the initial optimization on the co-sensitization ratio with varying compositions of **RJ-C6** and **XY1b** dyes (1:1, 1.6:1, 3:1).

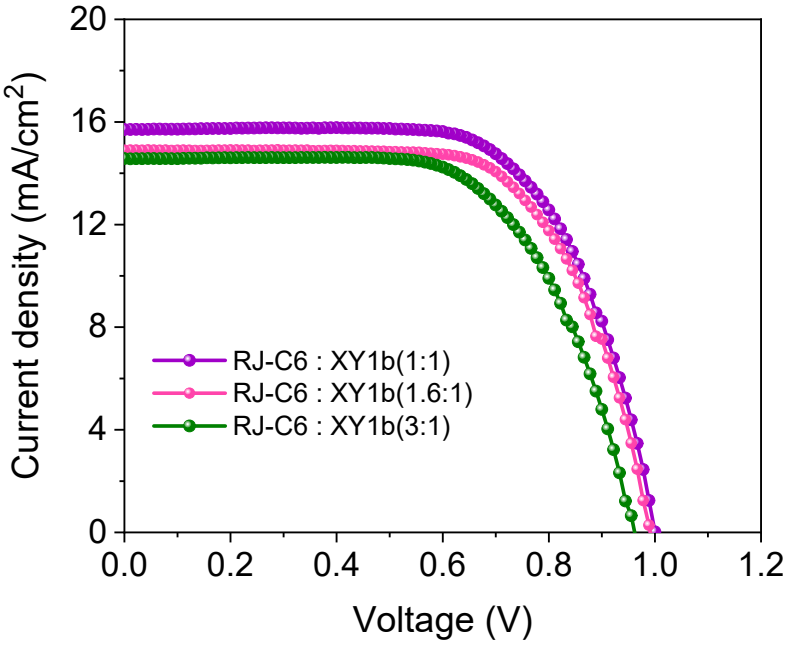

Table S5: *J-V* parameters under standard 1 sun illumination (AM 1.5 G, 100 mW/cm^2) corresponding to the initial optimization on the co-sensitization ratio with varying compositions of **RJ-C6** and **XY1b** dyes (1:1, 1.6:1, 3:1).

Device	V_{oc} (V)	J_{sc} (mA/cm^2)	*FF*	η (%)
RJ-C6:XY1b (1:1)	1.003 ± 0.005	15.71 ± 0.18	0.66 ± 0.005	10.39 ± 0.06
RJ-C6:XY1b (1.6:1)	0.996 ± 0.001	14.90 ± 0.11	0.67 ± 0.001	9.87 ±0.08
RJ-C6:XY1b (3:1)	0.966 ± 0.001	14.57 ± 0.05	0.64 ± 0.001	8.96 ±0.04

Fig. S14: *J-V* plot under standard 1000 lux WW CFL illumination (Input power – 283 µW/cm^2) of **XY1b** dye alone.

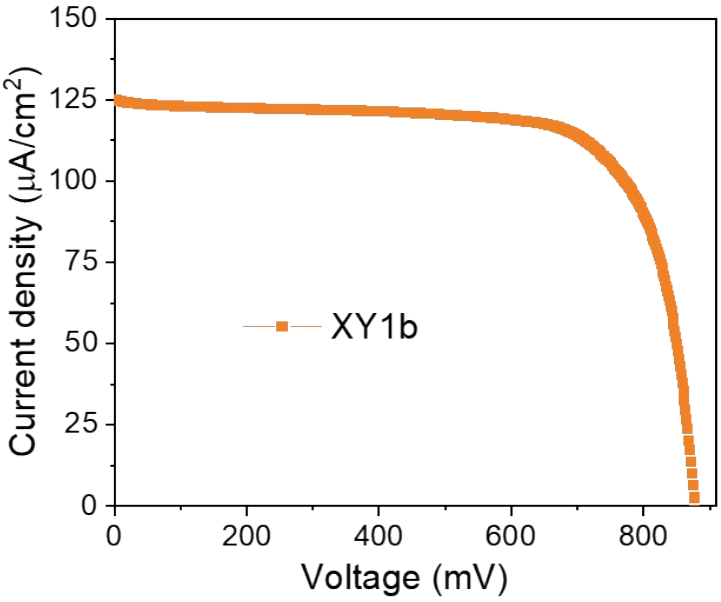

Table S6: *J-V* parameter under standard 1000 lux WW CFL illumination (input power – 283 µW/cm^2) of **XY1b** dye alone.

Device	V_{oc} (V)	J_{sc} (µA/cm^2)	*FF*	η (%)
XY1b	0.88±0.005	125.05±5.05	0.73±0.04	28.3±0.44

Fig. S15: Charge collection efficiency (η_{cc}) for **L0:XY1b, DN-F13:XY1b** and **RJ-C6:XY1b** co-sensitized DSCs using dual species copper (II/I) electrolyte.

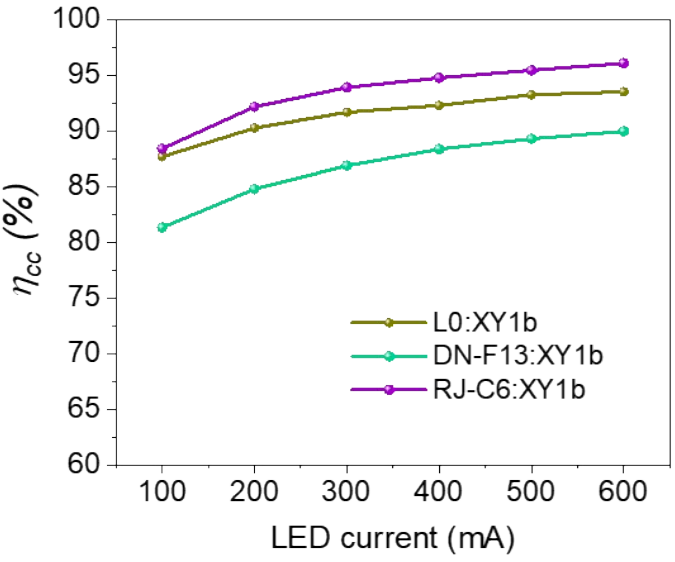

Fig. S16: Electron transport time measured using transient photocurrent decay (toolbox) method for varying co-sensitization composition ratio of **RJ-C6** and **XY1b** dyes (1:1, 1.6:1, 3:1) using dual species copper (II/I) electrolyte.

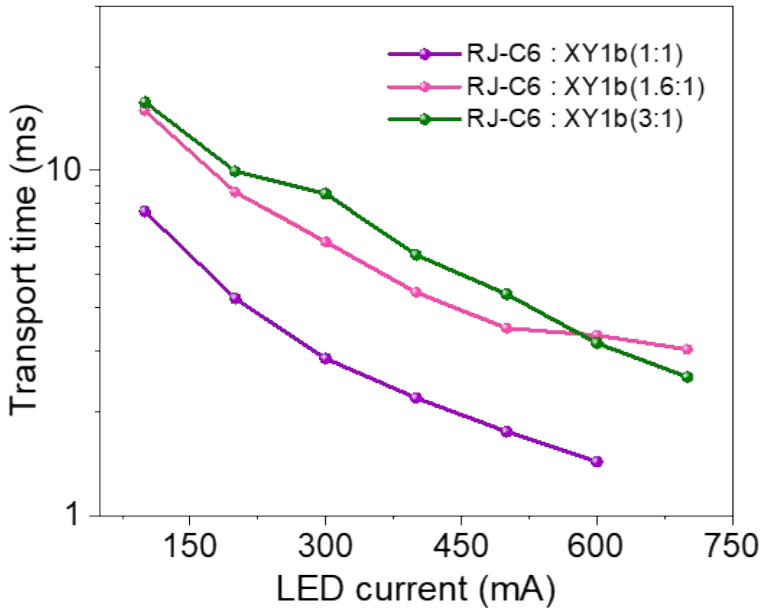

Fig. S17: Electron lifetime measured using open circuit voltage decay (OCVD) for varying co-sensitization composition ratio of **RJ-C6** and **XY1b** dyes (1:1, 1.6:1, 3:1) using dual species copper (II/I) electrolyte.

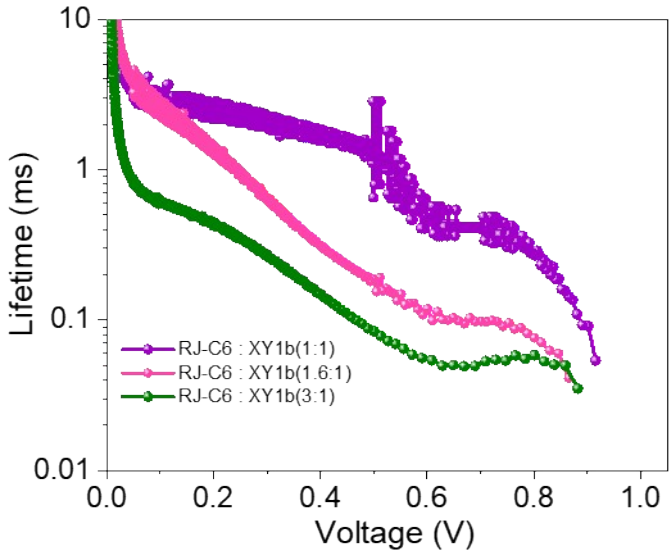

Fig. S18: Diffusion coefficient (D_n) for varying co-sensitization composition ratio of **RJ-C6** and **XY1b** dyes (1:1, 1.6:1, 3:1) using dual species copper (II/I) electrolyte.

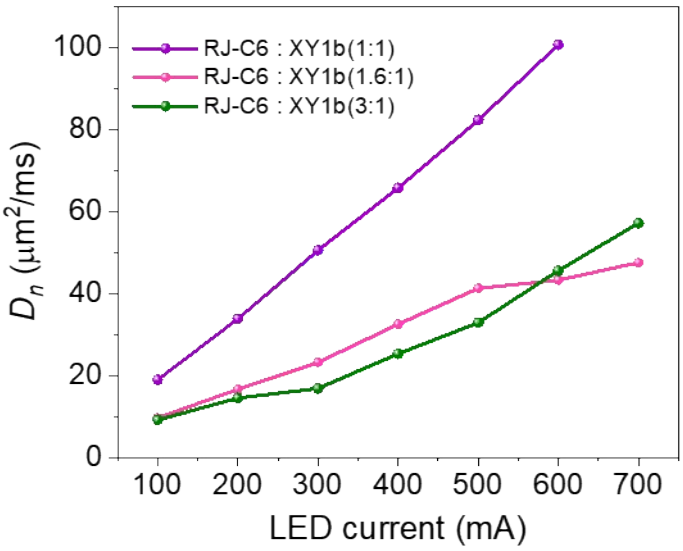

Fig. S19 Charge collection efficiency (η_{cc}) for varying co-sensitization composition ratio of **RJ-C6** and **XY1b** (1:1, 1.6:1, 3:1) using dual species copper (II/I) electrolyte.

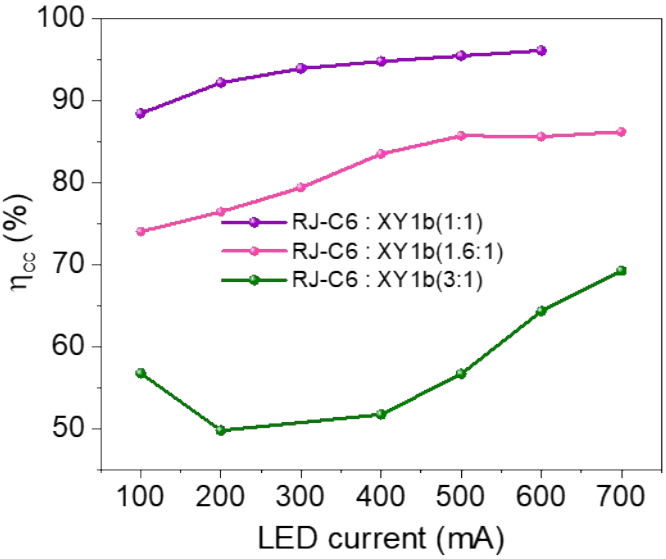

Fig. S20: EIS spectra under dark condition (voltage ~ V_{oc}) for **L0:XY1b, DN-F13:XY1b** and **RJ-C6:XY1b** co-sensitized DSCs using dual species copper (II/I) electrolyte.

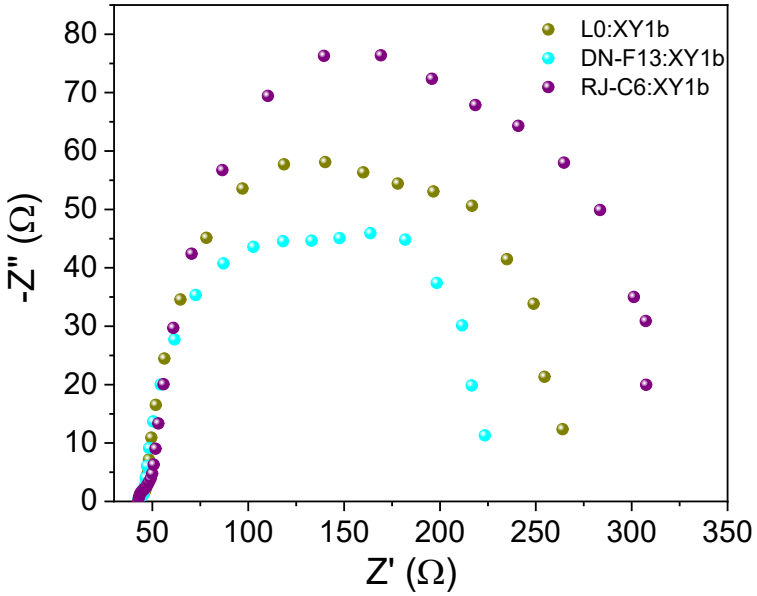

Fig. S21: IPCE response of **RJ-C6**:**XY1b** (1:1) co-senstized device and emission spectra of WW CFL (1000 lux) illumination.

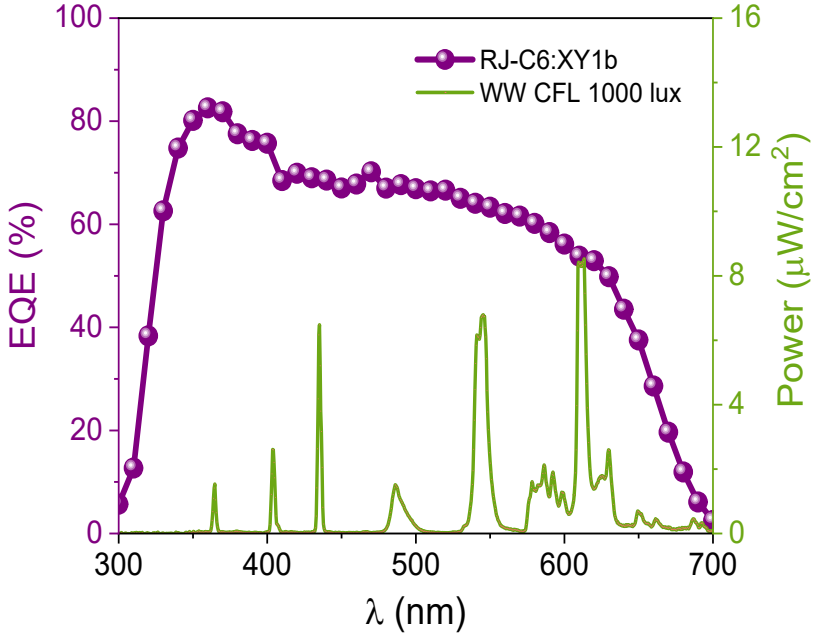

Fig. S22: Accelerated device stability for 800 hours under continuous LED light soaking at 80% relative humidity for **RJ-C6:XY1b (1:1)** co-sensitized devices using dual species copper (II/I) electrolyte.

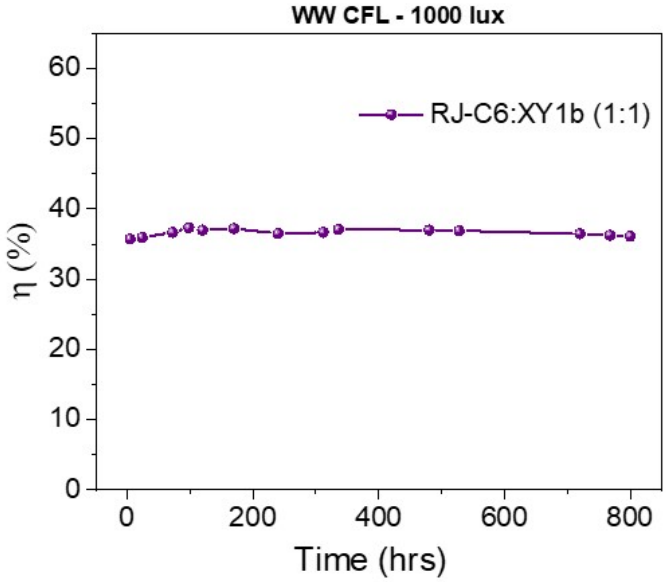

Fig. S23: Post-mortem analysis of **RJ-C6:XY1b** co-sensitized devices after 800 hrs stability test under continuous LED light soaking at 80% relative humidity – (a) *in-situ* IPCE profile and (b) *ex-situ* EIS under dark condition (voltage ~ V_{oc}).

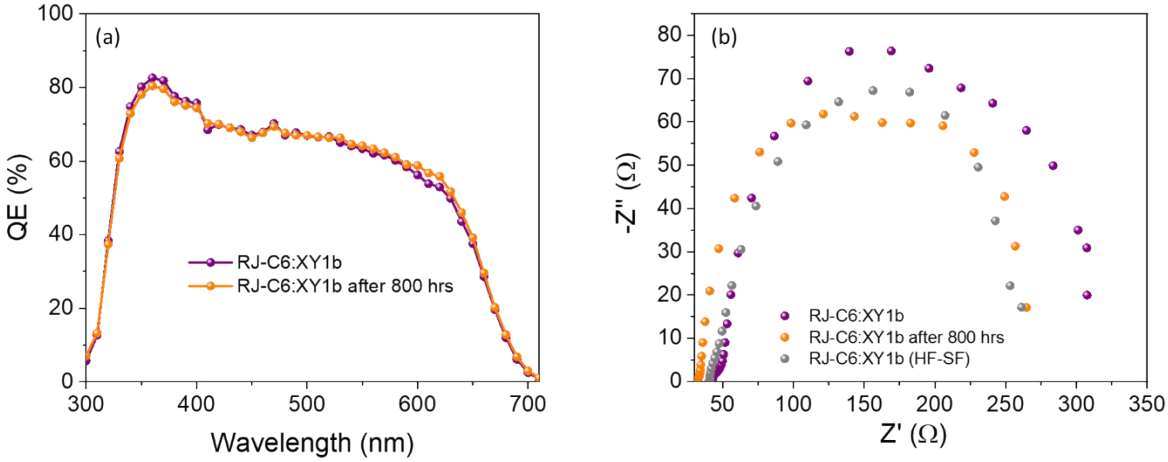

Fig. S24: The *J-V* plots obtained under WWCFL illumination intensities (ranging from 100 lux to 6000 lux: 100, 200, 500, 700, 1000, 2000, 3000, 4000, 5000, 6000 lux) for **RJ-C6:XY1b** co-sensitized devices with dual species copper (II/I) electrolyte.

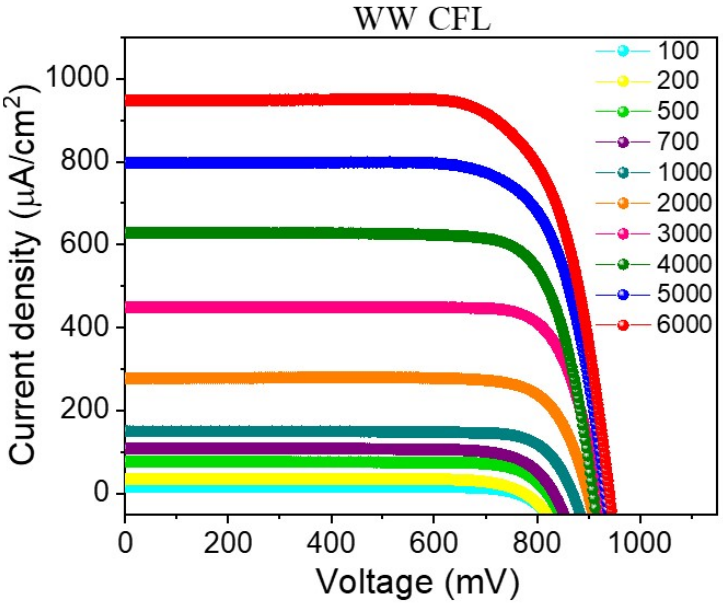

Table S7: Tabulated *J-V* parameters of the highest performing device in the batch obtained under warm white CFL illumination intensities (ranging from 100 lux to 6000 lux: 100, 200, 500, 700, 1000, 2000, 3000, 4000, 5000, 6000 lux) for **RJ-C6:XY1b** co-sensitized devices with dual species copper (II/I) electrolyte.

Light Intensity (lux)	P_{in} (μW/cm²)	V_{oc} (V)	J_{SC} (μA/cm²)	*FF*	η (%)	P_{out} (μW/cm²)
100	28.5	0.76	16.5	0.80	35.24	9.9
200	59.1	0.78	34.2	0.80	36.10	21.3
500	143.1	0.82	76.0	0.81	35.27	50.2
700	195.4	0.83	108.1	0.78	35.82	70.4
1000	283	0.87	149.7	0.81	37.28	105.6
2000	566	0.89	278.5	0.79	34.60	198.4
3000	849	0.92	449.6	0.81	39.46	333.2
4000	1130	0.91	628.4	0.79	39.98	451.3
5000	1415	0.93	797.2	0.75	39.30	557.1
6000	1698	0.94	948.8	0.73	38.34	651.7

Table S8: Comparison of the best photovoltaic results obtained using triphenylamine based co-sensitized dyes and dual species ($[Cu(dmp)_2]^+$/ $[Cu(dmp)_2Cl]^+$) from the present work with the best reported literature report using co-sensitized dyes under standard 1000 lux CFL illumination.

S No	J_{sc} (μA/cm²)	V_{oc} (mV)	*FF*	*η* (%)	Dye	Electrolyte	Reference
1	138.00	797.0	0.80	28.90	**D35:XY1**	$[Cu(tmby)_2]^{2+/+}$	Nat. Photonics, **2017**, 11, 372.
2	149.28	878.0	0.77	32.00	**Y123:XY1b**	$[Cu(tmby)_2]^{2+/+}$	Joule, **2018**, 2, 1108.
3	147.00	910.0	0.77	34.00	**L1:XY1**	$[Cu(tmby)_2]^{2+/+}$	Chem. Sci., **2020**, 11, 2895.
4	138.00	980.0	0.80	34.50	**MS5:X-Y1b**	$[Cu(tmby)_2]^{2+/+}$	Nat. Commun., **2021**, 12, 2.
5	134.90	905.3	0.80	35.60	**D35:XY1**	$[Cu(dmp)_2]^+$/ $[Cu(dmp)_2Cl]^+$	J. Mater. Chem. A, **2023**, 12, 1081.
6	149.70	870.0	0.80	**37.28**	**RJ-C6:XY1b**	$[Cu(dmp)_2]^+$/ $[Cu(dmp)_2Cl]^+$	**Present Work**

Table S9: Comparison of the highest photovoltaic efficiency for DSC obtained in the present study under 6000 Lux with the highest reported DSC efficiency in literature.

S. No	Light Intensity (Lux)	J_{sc} (μA/cm²)	V_{oc} (mV)	*FF*	*η* (%)	Dye	Electrolyte	Reference
1	6000	893.44	977.6	0.79	37.07	**CXC22**	$[Cu(dmp)_2]^{2+/+}$	Adv. Energy Mater. **2022**, 2104051
2	4000	628.40	910.0	0.79	**39.98**	**RJ-C6:XY1b**	$[Cu(dmp)_2]^+$/ $[Cu(dmp)_2Cl]^+$	**Present Work**

Fig. S25: A temperature sensor/clock (ACETEQ DC-2) powered using 2 serially interconnected DSCs (effective active area of 0.64 cm^2) fabricated using **RJ-C6**:**XY1b** co-sensitized dye combination and dual species $[Cu(II)(dmp)_2Cl]^+/[Cu(I)(dmp)_2]^{2+}$ electrolyte under indoor illumination approx. 1000 lux.

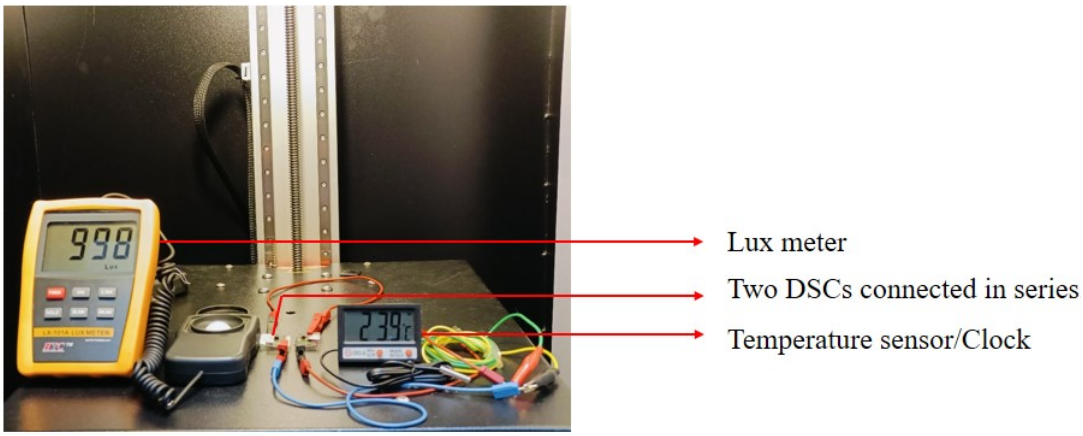

Section-VII. Reference

1 S. M. Meethal, S. C. Pradhan, J. Velore, S. Varughese, R. S. Pillai, F. Sauvage, A. Hagfeldt and S. Soman, *J. Mater. Chem. A*, 2023, **12**, 1081–1093.

2 R. Yuan, L. Zhang, L. Chen, H. Zhang, P. Dou, X. Ren, W. Chen, H. Zhou, Y. Wan and H. Wu, *Tetrahedron Lett.*, 2019, **60**, 1803–1807.

3 H. Zhou, Z. Wang, C. Gao, J. You and G. Gao, *Chem. Commun.*, 2013, **49**, 1832–1834.

4 N. Ganguly, S. Barik and S. Dutta, *Synthesis (Stuttg).*, 2011, **2011**, 828–828.

5 A. Jagadeesh, G. Veerappan, P. S. Devi, K. N. N. Unni and S. Soman, *J. Mater. Chem. A*, 2023, **11**, 14748–14759.

6 J. Velore, S. Chandra Pradhan, T. W. Hamann, A. Hagfeldt, K. N. N. Unni and S. Soman, *ACS Appl. Energy Mater.*, 2022, **5**, 2647–2654.

7 S. C. Pradhan, J. Velore, A. Hagfeldt and S. Soman, *J. Mater. Chem. C*, 2022, **10**, 3929–3936.

8 D. Zhang, M. Stojanovic, Y. Ren, Y. Cao, F. T. Eickemeyer, E. Socie, N. Vlachopoulos, J. E. Moser, S. M. Zakeeruddin, A. Hagfeldt and M. Grätzel, *Nat. Commun. 2021 121*, 2021, **12**, 1–10.

9 S. C. Pradhan and S. Soman, *Results in Surfaces and Interfaces*, 2021, **5**, 100030.